Chapter 8

Optimal control processes in active distribution networks

Mario Paolone, Jean-Yves Le Boudec, Konstantina Christakou and Dan-Cristian Tomozei

Typical optimal controls of power systems, such as scheduling of generators, voltage control, losses reduction, have been so far commonly investigated in the domain of high-voltage transmission networks. However, during the past years, the increased connection of distributed energy resources (DERs) in power distribution systems results in frequent violations of operational constraints in these networks and has raised the importance of developing optimal control strategies specifically applied to these systems (e.g., References 1–6). In particular, two of the most important control functionalities that have not yet been deployed in active distribution networks (ADNs)[1] are voltage control and lines congestion management [8]. Usually, this category of problems has been treated in the literature by means of linear approaches applied to the dependency between voltages and power flows as a function of the power injections, e.g., References 4, 6, 9, 10.

On the one hand, recent progress in information and communication technologies, the introduction of new advanced metering devices (see Chapter 3) such as phasor measurement units and the development of real-time state estimation algorithms (see Chapter 6) present new opportunities and will, eventually, enable the deployment of processes for *optimal* voltage control and lines congestion management in distribution networks.

On the other hand, ADNs exhibit specific peculiarities that render the design of such controls compelling. In particular, it is worth noting that the solution of optimal problems becomes of interest only if it meets the stringent time constraints required by real-time controls and imposed by the stochasticity of DERs, in particular photovoltaic units (PVs), largely present in these networks. Moreover, control schemes are meaningful for implementation in real-time controllers only when convergence to

[1]As defined in Reference 7, the term ADNs has emerged to define power distribution grids that have systems in place to control a combination of DERs, defined as generators, loads and storage. Distribution network operators (DNOs) have the possibility of managing the electricity flows using a flexible network topology. DERs take some degree of responsibility for system support, which will depend on a suitable regulatory environment and connection agreement.

an optimal solution is guaranteed. Finally, control processes for ADNs need to take into account the inherent multi-phase and unbalanced nature of these networks, as well as the non-negligible R/X ratio of longitudinal parameters of the medium and low-voltage lines, e.g., References 11, 12, together with the influence of transverse capacitances.[2] Taking into consideration the aforementioned requirements, the distribution management systems (DMSs) need to be updated accordingly in order to incorporate optimization processes for the scheduling of the DERs [13].

This chapter starts with a general description of a centralized DMS architecture that includes voltage control and lines congestion management functionalities. Then, the formulation of the corresponding optimal control problems is described, based on a linearized approach linking control variables, e.g., power injections, transformers tap positions, and controlled quantities, e.g., voltages, current flows, by means of sensitivity coefficients. Computation processes for these sensitivity coefficients are presented in Sections 8.2 and 8.3. Finally, in Section 8.4, we provide case studies of optimal voltage control and lines congestion management targeting IEEE distribution reference networks suitably modified to integrate distributed generation.

8.1 Typical architecture of ADN grid controllers

8.1.1 Control architecture

Throughout this chapter, we consider an ADN equipped with a number of distributed controllable energy resources, a monitoring infrastructure that provides the DNO with field measurements and a centralized DMS adapted from Reference 13. The architecture of the considered DMS is shown in Figure 8.1.

Its main modules are the following:

- **State estimation**: The first step towards the development of optimal control schemes for ADNs is the knowledge of the system state. To this end, the state estimation (SE) module involves algorithms that process field measurements and provide the DNO with the state of the grid, i.e., the voltage phasors at the network buses. It is worth noting that control functionalities in distribution systems can be characterized by dynamics in the order of few seconds, since they might be associated to the dynamics of renewable energy resources (RERs), e.g., Reference 14. In this respect, we consider the presence of a real-time state estimator (RTSE) capable of assessing the ADNs' state within few tens/hundreds of milliseconds with relatively high levels of accuracy and refresh rate (e.g., Reference 15). Provided that the network admittance matrix is known, once the voltage phasors are obtained, the computation of the nodal power injections, as well as the flows of each line, is straightforward.

[2]Note that line shunt parameters are non-negligible in case of networks characterized by the presence of coaxial cables. These types of components are typical, for instance, in the context of urban distribution networks.

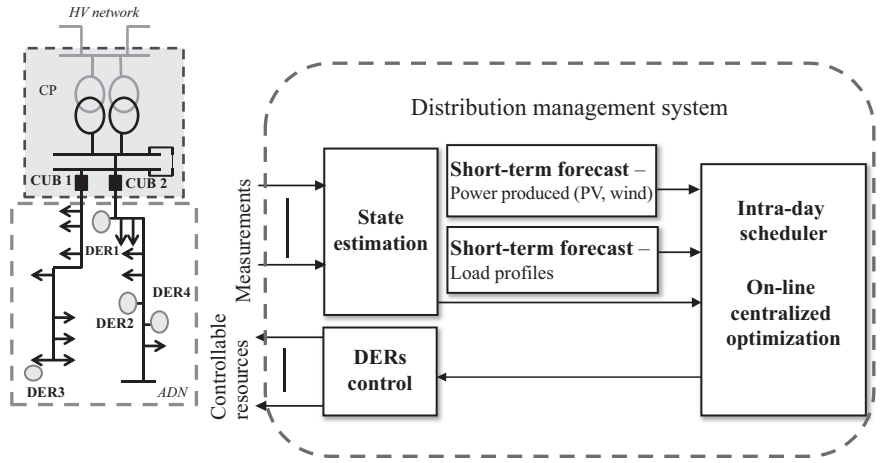

Figure 8.1 Distribution management system adopted for the proposed centralized controller

- **Short-term forecasts**:[3] This DMS module incorporates algorithms that are able to provide ultra-short-term forecasts for both the loads' consumption and the RERs' production, e.g., Reference 14. ADNs are characterized by increased penetration of highly volatile RERs. Therefore, the possibility to forecast as accurately as possible their power production can play a fundamental role, especially in cases where the RERs are requested to contribute to grid ancillary services. In the same direction, load forecasting is crucial especially in cases when demand-response actions are included in the control functionalities. This module is also useful in cases where multi-horizon optimization is used for the grid control, e.g., model predictive control [16], or uncertainty in loads and RERs' production is included in the control via, for instance, a robust optimization framework [17].
- **Intra-day scheduler and DERs control**: The intra-day scheduler module essentially comprises the real-time controller that acts in short-time intervals – in the order of few seconds to several minutes according to the control application. It uses the system state and the available short-term forecasts as inputs and formulates an optimization problem in order to obtain the optimal required power adjustments and the optimal variations in the under-load tap changers (ULTCs) positions which lead to the desired operation set point. Depending on the control application that the DNO wishes to implement, the objective function is modified accordingly. Typical examples of controls include resistive losses minimization, voltage deviations minimization, lines congestion management or energy supply cost minimization. Once the optimal set points are computed the DERs control module is responsible to communicate them to the controllable DERs.

[3]This functionality is of importance for energy management purposes. It is here mentioned for the sake of completeness but it is not used in the rest of the chapter.

In our case, the DNO is interested in minimizing the voltage deviations from the network-rated value and in maintaining the line current flows below their ampacity limits. In the following section, we focus on the actions that the online centralized controller performs to achieve these objectives.

8.1.2 Controller's actions

In what follows, the modules of state estimation, online centralized optimization and DERs control (see Figure 8.1) are adopted to formulate the control problem.

A network is considered composed of N_b buses, N_l lines and N_{DER} controllable resources. The rated value of the network voltage is denoted by V_o. The DNO wishes to compute the optimal DERs' active and reactive power variations (ΔP_i, ΔQ_i, $i = 1, \ldots, N_{DER}$), and the optimal ULTC positions Δn of the transformer interfacing the targeted ADN with the upper power grid layer[4] to achieve primary voltage control and lines congestion management.

To guarantee convergence to an optimal solution and enable fast implementation of the control scheme in real-time controllers, we use a linearized approach to formulate the optimal control problem. The first step towards this direction is to linearize the dependencies of the voltage and line currents with respect to the nodal power injections and ULTC positions. With this aim, at each time step t, the DNO uses the network state computed by the SE module, i.e., the phase-to-ground voltage phasors $\bar{V}_i$ at each bus i (e.g., References 18, 19) and, as a consequence, the branch current $\bar{I}_{ij}$ flowing from bus i to bus j.[5] To introduce the problem, we here make reference to direct sequence quantities. The extension to unbalanced three-phase systems is proposed in Section 8.3. Also, we assume that the system model, namely, the network admittance matrix, $[\bar{\boldsymbol{Y}}]$ is known. Using this information, the DNO can compute, subsequently, the values of the voltage and current sensitivity coefficients with respect to absorbed/injected power of a bus l where a controllable resource is connected, as well as with respect to the transformer's ULTC positions:

$$K_{P_{i,l}} := \frac{\partial |\bar{V}_i|}{\partial P_l}, \quad K_{Q_{i,l}} := \frac{\partial |\bar{V}_i|}{\partial Q_l}$$

$$\bar{H}_{P_{ij,l}} := \frac{\partial \bar{I}_{ij}}{\partial P_l}, \quad \bar{H}_{Q_{ij,l}} := \frac{\partial \bar{I}_{ij}}{\partial Q_l}$$

$$K_{n_i} := \frac{\partial |\bar{V}_i|}{\partial V_o}, \quad \bar{H}_{n_k} := \frac{\partial \bar{I}_{ij}}{\partial V_o}$$

[4]Note that we assume that transformer's ULTC is located in correspondence with the slack buses of the network because for distribution networks these represent the connections to external transmission or sub-transmission networks.

[5]In the rest of the chapter, complex numbers are denoted with a bar above (e.g., $\bar{V}$) and complex conjugates with a bar below (e.g., $\underline{V}$).

These sensitivities can be computed online by solving a linear system of equations (e.g., Reference 12). The details related to the computation of the sensitivities will be discussed in the following section.

Therefore, the following linear relations between variation in bus voltages, line currents and variations of active/reactive power $\Delta P_i, \Delta Q_i$ and ULTC $\boldsymbol{\Delta n}$ can be derived:

$$\begin{aligned}\Delta|\bar{V}|_i &\approx \boldsymbol{K_{P_i}}\boldsymbol{\Delta P} + \boldsymbol{K_{Q_i}}\boldsymbol{\Delta Q} + \boldsymbol{K_n}\boldsymbol{\Delta n} \triangleq (\boldsymbol{K_{P,Q,n}}\boldsymbol{\Delta(P,Q,n)})_i \\ \Delta\bar{I}_{ij} &\approx \bar{\boldsymbol{H}}_{\boldsymbol{P}_{ij}}\boldsymbol{\Delta P} + \bar{\boldsymbol{H}}_{\boldsymbol{Q}_{ij}}\boldsymbol{\Delta Q} + \bar{\boldsymbol{H}}_{\boldsymbol{n}}\boldsymbol{\Delta n} \triangleq (\bar{\boldsymbol{H}}_{\boldsymbol{P,Q,n}}\boldsymbol{\Delta(P,Q,n)})_{ij}\end{aligned}$$

where

$$\begin{aligned}\boldsymbol{K_{P_i}} &= \left[K_{P_{i,1}}, \ldots, K_{P_{i,N_{DER}}}\right] \\ \boldsymbol{K_{Q_i}} &= \left[K_{Q_{i,1}}, \ldots, K_{Q_{i,N_{DER}}}\right] \\ \boldsymbol{K_n} &= \left[K_{n_1}, \ldots, K_{n_{N_b}}\right] \\ \bar{\boldsymbol{H}}_{\boldsymbol{P}_{ij}} &= \left[\bar{H}_{P_{ij,1}}, \ldots, \bar{H}_{P_{ij,N_{DER}}}\right] \\ \bar{\boldsymbol{H}}_{\boldsymbol{Q}_{ij}} &= \left[\bar{H}_{Q_{ij,1}}, \ldots, \bar{H}_{Q_{ij,N_{DER}}}\right] \\ \bar{\boldsymbol{H}}_{\boldsymbol{n}} &= \left[\bar{H}_{n_1}, \ldots, \bar{H}_{n_{N_l}}\right]\end{aligned}$$

Using the sensitivity coefficients $\boldsymbol{K_{P,Q,n}}$ and $\bar{\boldsymbol{H}}_{\boldsymbol{P,Q,n}}$, the DNO can compute the optimal required power adjustments in the buses and the optimal ULTC positions $\{\boldsymbol{\Delta(P,Q,n)}^*\}$ which lead to the desired operation set point for optimal grid control. Depending on the grid's needs, the DNO can consider different objective functions. In this chapter, we assume that, at a given time step t, the DNO wishes to minimize the deviations of the voltage magnitudes in the network buses from the network-rated value, V_o, while keeping the line current flows below the ampacity limits, via the following constrained optimization problem (e.g., Reference 20):

$$\min_{\boldsymbol{\Delta(P,Q,n)}} \sum_i [(|\bar{V}_i| + (\boldsymbol{K_{P,Q,n}}\boldsymbol{\Delta(P,Q,n)})_i - |V_o|)^2 - \gamma^2]^+ \tag{8.1}$$

$$\text{subject to:} \quad |\bar{I}_{ij} + (\bar{\boldsymbol{H}}_{\boldsymbol{P,Q,n}}\boldsymbol{\Delta(P,Q,n)})_{ij}| \leq I_{max}, \;\; i,j = 1, \ldots, N_b, \; i \neq j \tag{8.2}$$

$$(P_j, Q_j) \in \mathcal{H}_j, \;\; j = 1, \ldots, N_{DER} \tag{8.3}$$

$$n_{min} \leq n \leq n_{max} \tag{8.4}$$

where we have used the notation $[a]^+ \triangleq max(a, 0)$. The constant γ in (8.1) represents the voltage threshold which defines the ranges outside of which the controller optimizes the voltage magnitudes. This avoids the minimization of the voltage deviations when they are within acceptable limits imposed by the DNO. Constraints (8.2) are the ampacity limits imposed on the line current flows. Constraints (8.3) represent the capability curves of the controllable resources. The last constraint (8.4) represents the minimum and maximum ULTC positions allowed.

Note that the formulation of the optimization problem in (8.1)–(8.4) is sufficiently generic. Indeed, according to the DNO's desire, the control problem can be modified to account for additional operational objectives. Also, in case the ULTCs are included in the control the problem becomes a mixed integer one, otherwise the corresponding sensitivity coefficients can be set to zero and control is achieved only through the scheduling of the DERs. In all cases, the key element for the formulation and solution of the linearized control problem is the computation of the sensitivity coefficients. With this aim, in the following sections, we recall the traditional way to compute sensitivity coefficients and we propose a method for the analytic derivation of these sensitivities, that is suitable for real-time network controllers.

8.2 Classic computation of sensitivity coefficients in power networks

Traditionally, there are two possible ways to calculate the sensitivity coefficients of our interest. The first method consists of estimating them by a series of load-flow calculations each performed for a small variation of a single control variable, i.e., nodal power injections, P_l, Q_l [6]:[6]

$$\begin{aligned}
\frac{\partial|\bar{V}_i|}{\partial P_l} &= \frac{\Delta|\bar{V}_i|}{\Delta P_l}\bigg|_{\substack{\Delta P_{i,i\neq l}=0\\ \Delta Q_{i,i\neq l}=0}} \qquad \frac{\partial|\bar{I}_{ij}|}{\partial P_l} = \frac{\Delta|\bar{I}_{ij}|}{\Delta P_l}\bigg|_{\substack{\Delta P_{i,i\neq l}=0\\ \Delta Q_{i,i\neq l}=0}} \\
\frac{\partial|\bar{V}_i|}{\partial Q_l} &= \frac{\Delta|\bar{V}_i|}{\Delta Q_l}\bigg|_{\substack{\Delta P_{i,i\neq l}=0\\ \Delta Q_{i,i\neq l}=0}} \qquad \frac{\partial|\bar{I}_{ij}|}{\partial Q_l} = \frac{\Delta|\bar{I}_{ij}|}{\Delta Q_l}\bigg|_{\substack{\Delta P_{i,i\neq l}=0\\ \Delta Q_{i,i\neq l}=0}}
\end{aligned} \tag{8.5}$$

where $\bar{V}_i$ is the direct sequence phase-to-ground voltage of bus i and $\bar{I}_{ij}$ is the direct sequence current flow between buses i and j ($i, j \in \{1, \ldots, N_b\}$).

It is worth observing that such a method is computationally expensive as it entails several consecutive load-flow computations even for a small number of controllable power injections. Therefore, it cannot be adopted, in principle, for real-time implementation.

The second method uses the Newton–Raphson (NR) formulation of the load-flow calculation to directly infer the voltage sensitivity coefficients as sub-matrices of the inverted Jacobian matrix (e.g., References 21–25). Assuming that all the network buses are constant PQ-injection buses, no voltage-controlled bus is present in the

[6]Note that, in what follows, we refer to the sensitivities of the current-flow magnitude with respect to active and reactive power injections as these quantities are real and they will be used for validation purposes and not to the complex quantities used in (8.1).

network and there is one slack bus in the system, the Jacobian matrix of the NR has the following form:

$$\boldsymbol{J} = \begin{bmatrix} \boldsymbol{J}_{PV} & \boldsymbol{J}_{P\delta} \\ \boldsymbol{J}_{QV} & \boldsymbol{J}_{Q\delta} \end{bmatrix} = \begin{bmatrix} \dfrac{\partial \boldsymbol{P}}{\partial |\bar{\boldsymbol{V}}|} & \dfrac{\partial \boldsymbol{P}}{\partial \boldsymbol{\delta}} \\ \dfrac{\partial \boldsymbol{Q}}{\partial |\bar{\boldsymbol{V}}|} & \dfrac{\partial \boldsymbol{Q}}{\partial \boldsymbol{\delta}} \end{bmatrix} \tag{8.6}$$

where $\boldsymbol{P}, \boldsymbol{Q}$ are the vectors of active and reactive nodal power injections/absorptions, and $|\bar{\boldsymbol{V}}|, \boldsymbol{\delta}$ are the magnitude and phase angle of the phase-to-ground voltage phasors. The elements of $\boldsymbol{J}$, i.e., the variation of the nodal active and reactive power injections as a function of the voltage magnitude and phase variations, are computed starting from the well-known non-linear power-flow equations. The detailed representation of these derivatives is given in (6.58)–(6.65) in Chapter 6.

The aforementioned Jacobian matrix, $\boldsymbol{J}$, is used in each iteration of the NR algorithm in order to linearly express the variations of active and reactive power as a function of the variations of the voltage magnitude and angles, in the following way:

$$\begin{bmatrix} \Delta \boldsymbol{P} \\ \Delta \boldsymbol{Q} \end{bmatrix} = \begin{bmatrix} \boldsymbol{J}_{PV} & \boldsymbol{J}_{P\delta} \\ \boldsymbol{J}_{QV} & \boldsymbol{J}_{Q\delta} \end{bmatrix} \times \begin{bmatrix} \Delta |\bar{\boldsymbol{V}}| \\ \Delta \boldsymbol{\delta} \end{bmatrix} \tag{8.7}$$

In our case, we are interested in the opposite link, namely expressing the variations of the voltage magnitude as a function of the active and reactive variations in the buses. This can be obtained in a straightforward manner, by inverting the Jacobian matrix:

$$\begin{bmatrix} \Delta |\bar{\boldsymbol{V}}| \\ \Delta \boldsymbol{\delta} \end{bmatrix} = \begin{bmatrix} \boldsymbol{J}_{PV} & \boldsymbol{J}_{P\delta} \\ \boldsymbol{J}_{QV} & \boldsymbol{J}_{Q\delta} \end{bmatrix}^{-1} \times \begin{bmatrix} \Delta \boldsymbol{P} \\ \Delta \boldsymbol{Q} \end{bmatrix} \tag{8.8}$$

At this point it is important to note that $\boldsymbol{J}$ is the Jacobian matrix of the whole network and that it also contains the elements corresponding to voltage angles. However, the optimal control problem as formulated in (8.1) requires only the sensitivities that correspond to specific controllable nodal injections and not the elements related to voltage angles. Therefore, the desired sensitivities correspond to sub-matrices of the inverted Jacobian matrix that need to be properly extracted.

It is worth observing that such a method does not allow to compute the sensitivities against the transformer's ULTC positions. Additionally, as known, the sub-matrix $\frac{\partial \boldsymbol{Q}}{\partial |\bar{\boldsymbol{V}}|}$ is usually adopted to express voltage variations as a function of reactive power injections when the ratio of longitudinal line resistance versus reactance is negligible. It is worth noting that such an assumption is no longer applicable to distribution systems that require, in addition, to take into account active power injections (e.g., Reference 26). Finally, such a method can be computationally expensive for very large networks. In these cases, this method requires the inversion of a large Jacobian matrix simply to extract a few columns corresponding to the controllable resources' power injections.

To overcome the aforementioned limitations, an efficient method for the computation of the desired sensitivities is given in the following section based on Reference 12.

8.3 Efficient computation of sensitivity coefficients of bus voltages and line currents in unbalanced radial electrical distribution networks

8.3.1 Voltage sensitivity coefficients

The analysis starts with the exact computation of the voltage sensitivity coefficients as a function of the network admittance matrix and its state. To this end, we derive mathematical expressions that link bus voltages to bus active and reactive power injections. For this purpose, a N_b-bus three-phase generic electrical network is considered. The following analysis treats each phase of the network separately and, thus, it can be applied to unbalanced networks (i.e., even for networks that cannot be decomposed with sequence components).

As known, the equations that link the voltage of each phase of the buses to the corresponding injected current are in total $M = 3N_b$ and they are given by:

$$[\bar{\boldsymbol{I}}_{abc}] = [\bar{\boldsymbol{Y}}] \cdot [\bar{\boldsymbol{V}}_{abc}] \tag{8.9}$$

where $[\bar{\boldsymbol{I}}_{abc}] = [\bar{I}_1^{a,b,c}, \ldots, \bar{I}_{N_b}^{a,b,c}]^T$ and $[\bar{\boldsymbol{V}}_{abc}] = [\bar{V}_1^{a,b,c}, \ldots, \bar{V}_{N_b}^{a,b,c}]^T$. We denote by a, b, c the three network phases. The $[\bar{\boldsymbol{Y}}]$ matrix is the so-called compound admittance matrix (e.g., Reference 27) and is formed as described in Section 6.1.1.1 of Chapter 6.

In order to simplify the notation, in what follows we will assume the following correspondences: $[\bar{\boldsymbol{I}}_{abc}] = [\bar{I}_1, \ldots, \bar{I}_M]^T$, $[\bar{\boldsymbol{V}}_{abc}] = [\bar{V}_1, \ldots, \bar{V}_M]^T$. For the rest of the analysis, we will consider the network as composed of S slack buses (the set of slack buses is $\mathcal{S}$) and N buses (the set of non-slack buses is $\mathcal{N}$) with PQ injections (i.e., $\{1, 2, \ldots, M\} = \mathcal{S} \cup \mathcal{N}$, with $\mathcal{S} \cap \mathcal{N} = \emptyset$). The PQ injections are considered constant and independent of the voltage.

The link between power injections and bus voltages reads

$$\underline{S}_i = \underline{V}_i \sum_{j \in \mathcal{S} \cup \mathcal{N}} \bar{Y}_{ij} \bar{V}_j, \quad i \in \mathcal{N} \tag{8.10}$$

The derived system of equations (8.10) holds for all the phases of each bus of the network. Since the objective is to calculate the partial derivatives of the voltage magnitude over the active and reactive power injected in the other buses, we have to consider separately the slack bus of the system. As known, the assumptions for the slack bus equations are to keep its voltage constant and equal to the network-rated

value, by also fixing its phase equal to zero. Hence, for the three phases of the slack bus, it holds that:

$$\frac{\partial \bar{V}_i}{\partial P_l} = 0, \quad \forall i \in \mathcal{S} \tag{8.11}$$

At this point, by using (8.10) as a starting point, one can derive closed-form mathematical expressions to define and quantify voltage sensitivity coefficients with respect to active and reactive power variations in correspondence with the N_b buses of the network. To derive voltage sensitivity coefficients, the partial derivatives of the voltages with respect to the active and reactive power P_l and Q_l of a bus $l \in \mathcal{N}$ have to be computed. The partial derivatives with respect to active power satisfy the following system of equations:

$$\mathbb{1}_{\{i=l\}} = \frac{\partial \underline{V}_i}{\partial P_l} \sum_{j \in \mathcal{S} \cup \mathcal{N}} \bar{Y}_{ij} \bar{V}_j + \underline{V}_i \sum_{j \in \mathcal{N}} \bar{Y}_{ij} \frac{\partial \bar{V}_j}{\partial P_l} \tag{8.12}$$

where it has been taken into account that:

$$\frac{\partial \underline{S}_i}{\partial P_l} = \frac{\partial \{P_i - jQ_i\}}{\partial P_l} = \mathbb{1}_{\{i=l\}} \tag{8.13}$$

The system of equations (8.12) is not linear over complex numbers, but it is linear with respect to $\frac{\partial \bar{V}_i}{\partial P_l}, \frac{\partial \underline{V}_i}{\partial P_l}$; therefore, it is linear over real numbers with respect to rectangular coordinates. As we show next, it has a unique solution for radial networks and can therefore be used to compute the partial derivatives in rectangular coordinates to reduce the computational effort.

A similar system of equations holds for the sensitivity coefficients with respect to the injected reactive power Q_l. With the same reasoning, by taking into account that:

$$\frac{\partial \underline{S}_i}{\partial Q_l} = \frac{\partial \{P_i - jQ_i\}}{\partial Q_l} = -j\mathbb{1}_{\{i=l\}} \tag{8.14}$$

we obtain that:

$$-j\mathbb{1}_{\{i=l\}} = \frac{\partial \underline{V}_i}{\partial Q_l} \sum_{j \in \mathcal{S} \cup \mathcal{N}} \bar{Y}_{ij} \bar{V}_j + \underline{V}_i \sum_{j \in \mathcal{N}} \bar{Y}_{ij} \frac{\partial \bar{V}_j}{\partial Q_l} \tag{8.15}$$

By observing the above linear systems of equations (8.12) and (8.15), we can see that the matrix that needs to be inverted in order to solve the system is fixed independently of the power of the lth bus with respect to which we want to compute the partial derivatives. The only element that changes is the left-hand side of the equations.

Once $\frac{\partial \bar{V}_i}{\partial P_l}, \frac{\partial \underline{V}_i}{\partial P_l}$ are obtained, the partial derivatives of the voltage magnitude can be expressed as:

$$\frac{\partial |\bar{V}_i|}{\partial P_l} = \frac{1}{|\bar{V}_i|} Re\left(\underline{V}_i \frac{\partial \bar{V}_i}{\partial P_l} \right) \tag{8.16}$$

and similar equations hold for derivatives with respect to reactive power injections.

Theorem 8.1. *The system of equations (8.12), where l is fixed and the unknowns are $\frac{\partial \bar{V}_i}{\partial P_l}$, $i \in \mathcal{N}$, has a unique solution for every radial electrical network and for any operating point $(\bar{\boldsymbol{V}}, \bar{\boldsymbol{S}})$ where the load-flow Jacobian is invertible. The same holds for the system of equations (8.15), where the unknowns are $\frac{\partial \bar{V}_i}{\partial Q_l}$, $i \in \mathcal{N}$.*

Proof. Since the system is linear with respect to rectangular coordinates and there are as many unknowns as equations, the theorem is equivalent to showing that the corresponding homogeneous system of equations has only the trivial solution. The homogeneous system can be written as:

$$0 = \underline{\Delta}_i \sum_{j \in \mathcal{S} \cup \mathcal{N}} \bar{Y}_{ij} \bar{V}_j + \underline{V}_i \sum_{j \in \mathcal{N}} \bar{Y}_{ij} \bar{\Delta}_j, \quad \forall i \in \mathcal{N} \tag{8.17}$$

where $\bar{\Delta}_i$ are the unknown complex numbers, defined for $i \in \mathcal{N}$. We want to show that $\bar{\Delta}_i = 0$ for all $i \in \mathcal{N}$. Let us consider two electrical networks with the same topology, i.e., same $[\bar{\boldsymbol{Y}}_{abc}]$ matrix, where the voltages are given. In the first network, the voltages are

$$\begin{aligned} \bar{V}'_i &= \bar{V}_i, && \forall i \in \mathcal{S} \\ \bar{V}'_i &= \bar{V}_i + \epsilon \bar{\Delta}_i, && \forall i \in \mathcal{N} \end{aligned} \tag{8.18}$$

and in the second network they are

$$\begin{aligned} \bar{V}''_i &= \bar{V}_i, && \forall i \in \mathcal{S} \\ \bar{V}''_i &= \bar{V}_i - \epsilon \bar{\Delta}_i, && \forall i \in \mathcal{N} \end{aligned} \tag{8.19}$$

where ϵ is a positive real number.

Let $\underline{S}'_i$ be the conjugate of the absorbed/injected power at the ith bus in the first network, and $\underline{S}''_i$ in the second. Apply (8.10) to bus $i \in \mathcal{N}$ in the first network:

$$\begin{aligned} \underline{S}'_i &= \underline{V}'_i \sum_{j \in \mathcal{S} \cup \mathcal{N}} \bar{Y}_{ij} \bar{V}'_j \\ &= (\underline{V}_i + \epsilon \underline{\Delta}_i) \left(\sum_{j \in \mathcal{S}} \bar{Y}_{ij} \bar{V}_j + \sum_{j \in \mathcal{N}} \bar{Y}_{ij} (\bar{V}_j + \epsilon \bar{\Delta}_j) \right) \\ &= \underline{V}_i \sum_{j \in \mathcal{S} \cup \mathcal{N}} \bar{Y}_{ij} \bar{V}_j + \epsilon^2 \underline{\Delta}_i \sum_{j \in \mathcal{N}} \bar{Y}_{ij} \bar{\Delta}_j + \epsilon \underline{\Delta}_i \sum_{j \in \mathcal{S} \cup \mathcal{N}} \bar{Y}_{ij} \bar{V}_j + \underline{V}_i \sum_{j \in \mathcal{N}} \bar{Y}_{ij} \epsilon \bar{\Delta}_j \end{aligned}$$

Similarly, for the second network and for all buses $i \in \mathcal{N}$:

$$\underline{S}''_i = \underline{V}_i \sum_{j \in \mathcal{S} \cup \mathcal{N}} \bar{Y}_{ij} \bar{V}_j + \epsilon^2 \underline{\Delta}_i \sum_{j \in \mathcal{N}} \bar{Y}_{ij} \bar{\Delta}_j - \epsilon \underline{\Delta}_i \sum_{j \in \mathcal{S} \cup \mathcal{N}} \bar{Y}_{ij} \bar{V}_j - \underline{V}_i \sum_{j \in \mathcal{N}} \bar{Y}_{ij} \epsilon \bar{\Delta}_j$$

Subtract the last two equations and obtain

$$\underline{S}_i' - \underline{S}_i'' = 2\epsilon \left(\underline{\Delta}_i \sum_{j \in \mathcal{S} \cup \mathcal{N}} \bar{Y}_{ij} \bar{V}_j + \underline{V}_i \sum_{j \in \mathcal{N}} \bar{Y}_{ij} \bar{\Delta}_j \right)$$

By (8.17), it follows that $\underline{S}_i' = \underline{S}_i''$ for all $i \in \mathcal{N}$. Thus, the two networks have the same active and reactive powers at all non-slack buses and the same voltages at all slack buses. As the load-flow Jacobian matrix is invertible according to Theorem 8.1 hypothesis, we can apply the inverse function theorem. As a consequence, the non-linear system of the power flow equations is locally invertible in a neighbourhood around the current operating point $(\bar{\boldsymbol{V}}, \bar{\boldsymbol{S}})$. Now, we take ϵ arbitrarily small, such that $\underline{V}_i'$ and $\underline{V}_i''$ belong to this neighbourhood where there is a one-to-one mapping between the powers and voltages. As the powers that correspond to $\underline{V}_i'$ and $\underline{V}_i''$ are exactly the same, then it follows that the voltage profile of these networks must be exactly the same, i.e., $\bar{V}_i - \epsilon \bar{\Delta}_i = \bar{V}_i + \epsilon \bar{\Delta}_i$ for all $i \in \mathcal{N}$ and thus $\bar{\Delta}_i = 0$ for all $i \in \mathcal{N}$. □

8.3.2 Current sensitivity coefficients

From the previous analysis, the sensitivity coefficients linking the power injections to the voltage variations are known. Thus, it is straightforward to express the branch current sensitivities with respect to the same power injections. Assuming to represent the lines that compose the network by means of π-model equivalents, the current flow $\bar{I}_{ij}$ between buses i and j can be expressed as a function of the phase-to-ground voltages of the relevant i,j buses as follows:

$$\bar{I}_{ij} = \bar{Y}_{ij}(\bar{V}_i - \bar{V}_j) + \bar{Y}_{i_0} \bar{V}_i \tag{8.20}$$

$$\bar{I}_{ji} = \bar{Y}_{ij}(\bar{V}_j - \bar{V}_i) + \bar{Y}_{j_0} \bar{V}_j \tag{8.21}$$

where $\bar{Y}_{ij}$ is the generic element of $[\bar{\boldsymbol{Y}}]$ matrix between bus i and bus j and $\bar{Y}_{i_0}$ is the shunt element on the receiving end of line $i - j$.

Since the voltages can be expressed as a function of the power injections into the network buses, the partial derivatives of the current with respect to the active and reactive power injections in the network can be expressed as:

$$\frac{\partial \bar{I}_{ij}}{\partial P_l} = \bar{Y}_{ij} \left(\frac{\partial \bar{V}_i}{\partial P_l} - \frac{\partial \bar{V}_j}{\partial P_l} \right) + \bar{Y}_{i_0} \left(\frac{\partial \bar{V}_i}{\partial P_l} \right), \quad \frac{\partial \bar{I}_{ij}}{\partial Q_l} = \bar{Y}_{ij} \left(\frac{\partial \bar{V}_i}{\partial Q_l} - \frac{\partial \bar{V}_j}{\partial Q_l} \right) + \bar{Y}_{i_0} \left(\frac{\partial \bar{V}_i}{\partial Q_l} \right) \tag{8.22}$$

$$\frac{\partial \bar{I}_{ji}}{\partial P_l} = \bar{Y}_{ij} \left(\frac{\partial \bar{V}_j}{\partial P_l} - \frac{\partial \bar{V}_i}{\partial P_l} \right) + \bar{Y}_{j_0} \left(\frac{\partial \bar{V}_j}{\partial P_l} \right), \quad \frac{\partial \bar{I}_{ji}}{\partial Q_l} = \bar{Y}_{ij} \left(\frac{\partial \bar{V}_j}{\partial Q_l} - \frac{\partial \bar{V}_i}{\partial Q_l} \right) + \bar{Y}_{j_0} \left(\frac{\partial \bar{V}_j}{\partial Q_l} \right) \tag{8.23}$$

Applying the same reasoning as earlier, the branch current sensitivity coefficients with respect to an active power P_l can be computed using the following expressions:

$$\frac{\partial|\bar{I}_{ij}|}{\partial P_l} = \frac{1}{|\bar{I}_{ij}|} Re\left(\underline{I}_{ij} \frac{\partial \bar{I}_{ij}}{\partial P_l}\right) \tag{8.24}$$

Similar expressions can be derived for the current coefficients with respect to the reactive power in the buses as:

$$\frac{\partial|\bar{I}_{ij}|}{\partial Q_l} = \frac{1}{|\bar{I}_{ij}|} Re\left(\underline{I}_{ij} \frac{\partial \bar{I}_{ij}}{\partial Q_l}\right) \tag{8.25}$$

8.3.3 Sensitivity coefficients with respect to transformer's ULTC

This subsection is devoted to the derivation of analytic expressions for the voltage sensitivity coefficients[7] with respect to tap positions of a transformer. We assume that transformers' tap changers are located in correspondence with the slack buses of the network as for distribution networks these represent the connections to external transmission or sub-transmission networks. As a consequence, the voltage sensitivities as a function of the tap positions are equivalent to the voltage sensitivities as a function of the slack reference voltage.[8] We assume that the transformers' voltage variations due to tap position changes are small enough so that the partial derivatives considered in the following analysis are meaningful. Furthermore, we assume that the power injections at the network buses are constant and independent of the voltage.

With the same reasoning as in Section 8.3.1, the analysis starts in (8.10). We write $\bar{V}_\ell = |\bar{V}_\ell| e^{j\delta_\ell}$ for all buses ℓ. For a bus $i \in \mathcal{N}$, the partial derivatives with respect to the voltage magnitude $|\bar{V}_k|$ of a slack bus $k \in \mathcal{S}$ are considered:

$$-\underline{V}_i \bar{Y}_{ik} e^{j\delta_k} = \underline{W}_{ik} \sum_{j \in \mathcal{S} \cup \mathcal{N}} \bar{Y}_{ij} \bar{V}_j + \underline{V}_i \sum_{j \in \mathcal{N}} \bar{Y}_{ij} \bar{W}_{jk} \tag{8.26}$$

where

$$\bar{W}_{ik} := \frac{\partial \bar{V}_i}{\partial |\bar{V}_k|} = \left(\frac{1}{|\bar{V}_i|} \frac{\partial |\bar{V}_i|}{\partial |\bar{V}_k|} + j \frac{\partial \delta_i}{\partial |\bar{V}_k|}\right) \bar{V}_i, \quad i \in \mathcal{N}$$

We have taken into account that:

$$\frac{\partial}{\partial |\bar{V}_k|} \sum_{j \in \mathcal{S}} \bar{Y}_{ij} \bar{V}_j = \bar{Y}_{ik} e^{j\delta_k} \tag{8.27}$$

[7]Note that as shown earlier once the voltage sensitivities are obtained, the ones of currents can be computed directly.

[8]It is worth noting that even if the ULTCs have phase-shifting capabilities, we do not compute the corresponding sensitivities. The reason is that we consider that ULTCs are located in correspondence with the slack bus of the network. Therefore, any shift in the slack bus voltage phase directly implies that all the voltage angles of the network buses rotate by the same quantity.

and

$$\frac{\partial \underline{S}_i}{\partial |\bar{V}_k|} = 0 \tag{8.28}$$

The derived system of equations (8.26) is linear with respect to $\underline{W}_{ik}$ and $\bar{W}_{ik}$, and has the same associated matrix as the system in (8.12). Since the resulting homogeneous system of equations is identical to the one in (8.17), by Theorem 8.1, it has a unique solution.

After resolution of (8.26), we find that the sensitivity coefficients with respect to the tap position of the transformer at bus k are given by

$$\frac{\partial |\bar{V}_i|}{\partial |\bar{V}_k|} = |\bar{V}_i| Re\left(\frac{\bar{W}_{ik}}{\bar{V}_i}\right) \tag{8.29}$$

8.4 Application examples

8.4.1 Distribution network case studies

Two IEEE distribution test feeders have been used for the validation of the proposed method and for its application to the problem of voltage control and lines congestion management. The first adopted feeder is the IEEE 34-bus distribution test feeder. Its topology is shown in Figure 8.2 and it is based on the original feeder in Reference 28. It is a three-phase feeder and consists of 34 buses where bus 1 is the slack bus. The assumed line-to-line Root Mean Square (RMS)-rated voltage is equal to 24.9 kV and the network base power is 2.5 MVA. The used line configuration is the #300 of Reference 28 for each line of the feeder. The values of the resistance, reactance and susceptance, as well as the line lengths are given in Appendix B.

Table 8.1 shows the active and reactive power consumption of the loads in the three phases of each network bus.

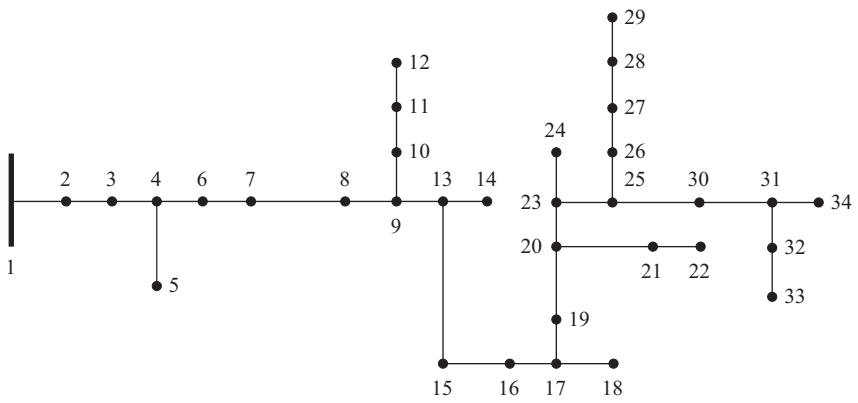

Figure 8.2 Adopted IEEE 34-bus distribution test feeder

Table 8.1 Load and generation data for the IEEE 34-bus distribution test feeder

Bus	P_α (kW)	Q_α (kvar)	P_β (kW)	Q_β (kvar)	P_c (kW)	Q_c (kvar)
1	0	0	0	0	0	0
2	0	0	−15	−7.5	−12.5	−7
3	0	0	0	0	0	0
4	0	0	0	0	0	0
5	0	0	−8	−4	0	0
6	0	0	0	0	0	0
7	0	0	0	0	0	0
8	0	0	0	0	0	0
9	0	0	0	0	0	0
10	0	0	0	0	0	0
11	−17	−8.5	0	0	0	0
12	−67.5	−35	0	0	0	0
13	0	0	−2.5	−1	0	0
14	0	0	−20	−10	0	0
15	0	0	0	0	−2	−1
16	−8.5	−4	−5	−2.5	−12.5	−5
17	0	0	0	0	0	0
18	25	0	25	0	25	0
19	0	0	0	0	0	0
20	0	0	0	0	0	0
21	0	0	0	0	0	0
22	−75	−37.5	−75	−37.5	−75	−37.5
23	25	0	25	0	25	0
24	25	0	25	0	25	0
25	2	−1	−7.5	−4	−6.5	−3.5
26	0	0	0	0	0	0
27	−72	−55	−67.5	−52.5	−67.5	−52.5
28	0	0	−12.5	−6	−10	−5.5
29	−10	−8	−21.5	−13.5	−10	−8
30	−18	−12	−20	−13	−65	−35.5
31	−15	−7.5	−5	−3	−21	−11
32	0	0	0	0	0	0
33	25	0	25	0	25	0
34	−13.5	−8	−15.5	−9	−4.5	−3.5

The same table gives the values of the active power injected by the DERs, installed in buses 18, 23, 24 and 33. The DERs do not inject any reactive power in the nominal case. We use the convention that negative values represent power consumption, whereas positive values power injection.

The second adopted feeder is the IEEE 13-bus distribution test feeder, shown in Figure 8.3. It is based as well on Reference 28. It is a three-phase feeder composed of 13 buses where bus 1 represents the connection to the sub-transmission network. The assumed network line-to-line RMS voltage is equal to 15 kV, the base power is 10 MVA and the lines are unbalanced. The used line configuration is the #602 of Reference 28 for each line of the feeder. The values of the resistance, reactance

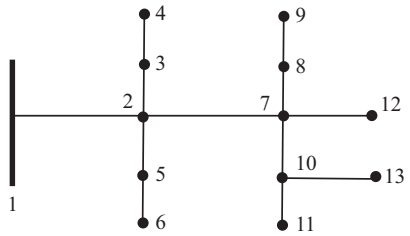

Figure 8.3 Adopted IEEE 13-bus distribution test feeder

Table 8.2 Load and generation data for the IEEE 13-bus distribution test feeder

Bus	P_α (kW)	Q_α (kvar)	P_β (kW)	Q_β (kvar)	P_c (kW)	Q_c (kvar)
1	0	0	0	0	0	0
2	−17	−10	−66	−38	−117	−68
3	0	0	0	0	0	0
4	−160	−110	−120	−90	−120	−90
5	0	0	−170	−125	0	0
6	0	0	−230	−132	0	0
7	−385	−220	−385	−220	−385	−220
8	0	0	0	0	−170	−151
9	−485	−190	−68	−60	−290	−212
10	0	0	0	0	0	0
11	0	0	0	0	−170	−80
12	0	0	0	0	0	0
13	−128	−86	0	0	0	0

and susceptance and the line lengths are given in Appendix B. The loads are also characterized by unbalanced power absorptions as can be observed in Table 8.2.

In the following sections, first the proposed method for the computation of the sensitivity coefficients is validated and then several application examples of voltage control and lines congestion management are shown.

8.4.2 Numerical validation

The numerical validation of the proposed method for the computation of voltage and current sensitivities is performed using the IEEE 13-bus test feeder and by using two different approaches. In particular, as the inverse of the load-flow Jacobian matrix provides the voltage sensitivities, the comparison reported below makes reference to such a method for the voltage sensitivities only. On the contrary, as the inverse of the load-flow Jacobian matrix does not provide current sensitivity coefficients, their accuracy is evaluated by using a numerical approach where the load-flow problem is solved by applying small injection perturbations into a given network (see Section 8.2). A similar approach is deployed to validate the sensitivities with respect to ULTC

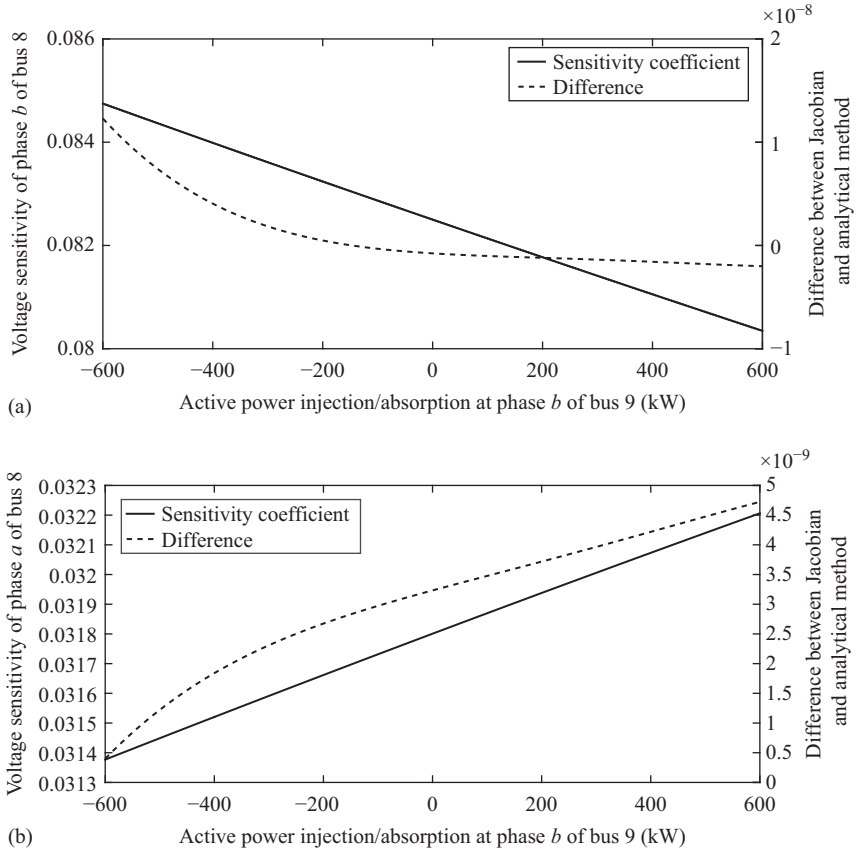

Figure 8.4 Voltage sensitivities of bus 8 as a function of active power injections at bus 9. (a) Voltage sensitivity of phase b of bus 8 with respect to active power injection at phase b of bus 9. (b) Voltage sensitivity of phase a of bus 8 with respect to active power injection at phase b of bus 9

positions of the transformers, i.e., small perturbations of the voltage magnitude of one phase of the slack bus and solution of the load-flow problem.

For brevity, we limit the validation of the proposed method to a reduced number of buses. In particular, we refer to the variation of voltages at bus 8 with respect to load/injection at bus 9:

$$\frac{\partial|\bar{V}_8^a|}{\partial P_9^b}, \quad \frac{\partial|\bar{V}_8^b|}{\partial P_9^b}, \quad \frac{\partial|\bar{V}_8^a|}{\partial Q_9^b}, \quad \frac{\partial|\bar{V}_8^b|}{\partial Q_9^b}$$

In Figure 8.4(a), the voltage sensitivity of phase *b* of bus 8 is shown with respect to active power absorption and generation at phase *b* of bus 9. Figure 8.4(b) shows

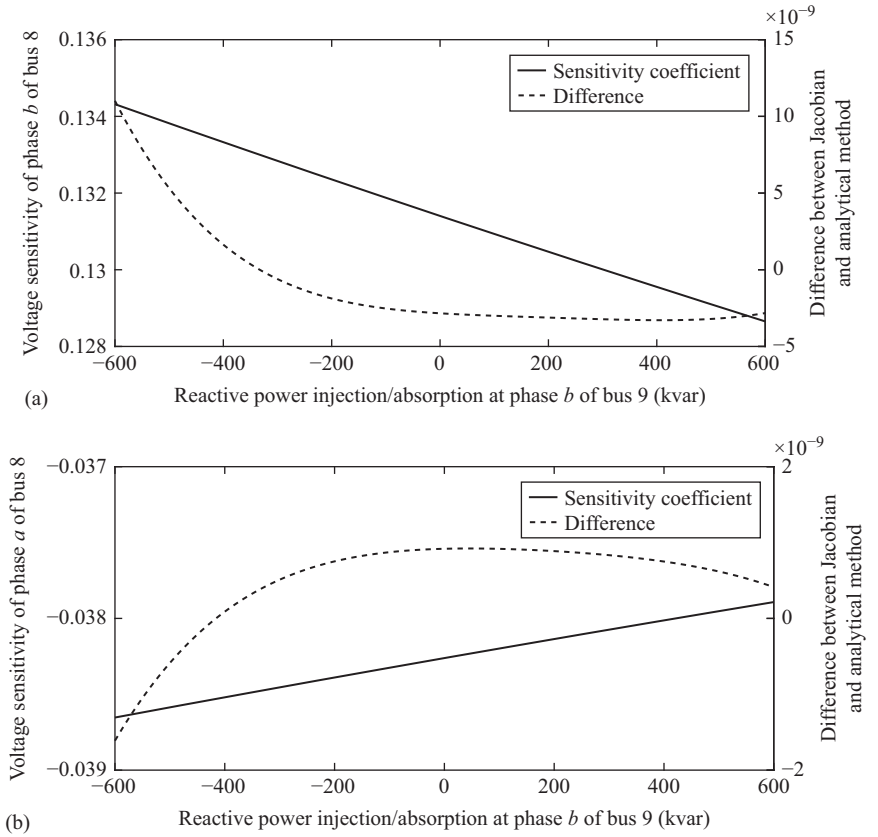

Figure 8.5 Voltage sensitivities of bus 8 as a function of reactive power injections at bus 9. (a) Voltage sensitivity of phase b of bus 8 with respect to reactive power injection at phase b of bus 9. (b) Voltage sensitivity of phase a of bus 8 with respect to reactive power injection at phase b of bus 9

for the same buses as Figure 8.4(b), same sensitivity but referring to voltage and power belonging to different phases. Additionally, Figure 8.5(a) and (b) shows the voltage sensitivity of bus 8 with respect to reactive power absorption and generation at bus 9. In all these four figures, the dashed line represents the difference between the traditional approach, i.e., based on the inverse of the Jacobian matrix, and the analytic method proposed here. As it can be observed, the overall differences are negligible, in the order of magnitude of 10^{-9}. In Figure 8.6(a) and (b), the current sensitivity coefficient of phase *a* of branch 10-13 is presented with respect to active and reactive power absorption/generation at phase *a* of bus 13. In the same figures, the dashed lines represent the difference between the analytic values and the numerical ones. Even for these coefficients extremely low errors are obtained, in the order of 10^{-5}.

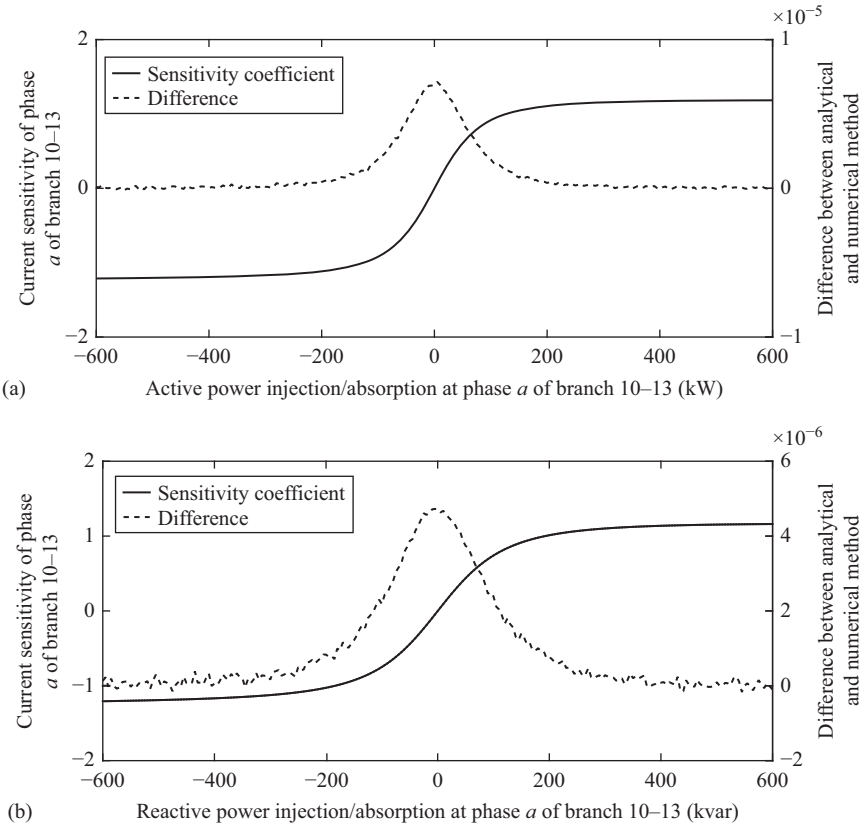

Figure 8.6 Current sensitivity of branch 10-13 as a function of power injections at bus 13. (a) Current sensitivity of phase a of branch 10-13 with respect to active power at phase a of bus 13. (b) Current sensitivity of phase a of branch 10-13 with respect to reactive power at phase a of bus 13

Concerning the validation of voltage sensitivities against tap-changer positions, we have made reference to the IEEE 13-bus test feeder where the slack bus and therefore the primary substation transformer is placed in correspondence with bus 1. We assume to vary the slack bus voltage of ±6% over 72 tap positions (where position "0" refers to the network-rated voltage). In Figure 8.7, the sensitivity of voltage in phase *a* of bus 7 is shown with respect to the tap positions in phases *a*, *b* and *c* of the slack. Also, in this case, the difference between the analytically inferred sensitivities and the numerical computed ones is negligible (i.e., in the order of magnitude of 10^{-6}).

It is worth observing that for the case of the voltage sensitivities, coefficients that refer to the voltage variation as a function of a perturbation (power injection or tap-changer position) of the same phase, show the largest coupling although a non-negligible cross dependency can be observed between different phases (see for instance Figures 8.4 and 8.5).

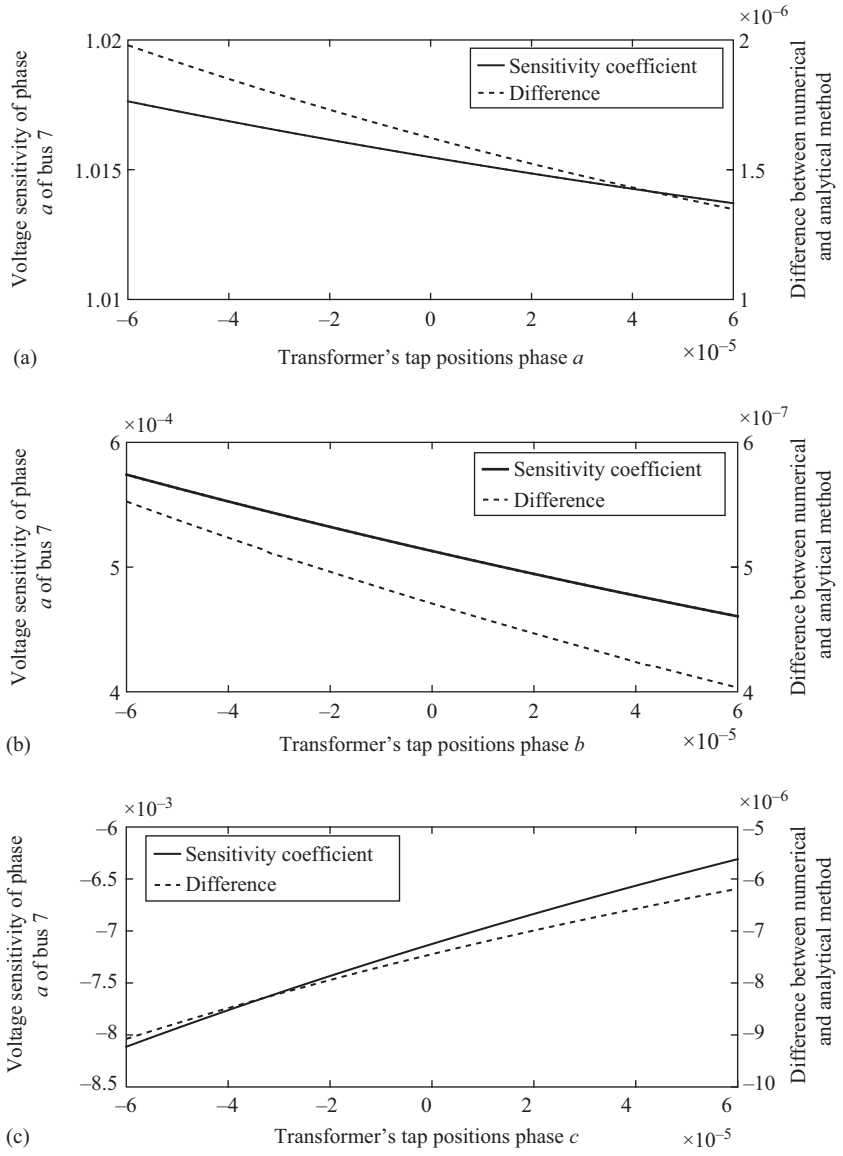

Figure 8.7 Voltage sensitivities of phase a of bus 7 as a function of transformer's ULTC positions. (a) Voltage sensitivity of phase a of bus 7 with respect to ULTC position at phase a of the slack bus. (b) Voltage sensitivity of phase a of bus 7 with respect to ULTC position at phase b of the slack bus. (c) Voltage sensitivity of phase a of bus 7 with respect to ULTC position at phase c of the slack bus

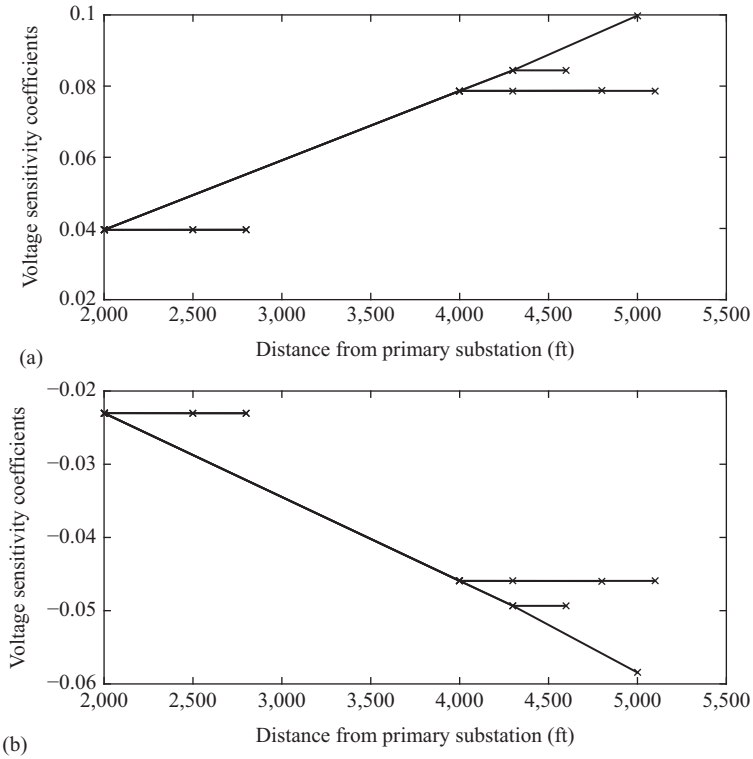

Figure 8.8 Voltage sensitivities with respect to active power absorption at bus 13 as a function of the distance from the slack bus. (a) Voltage sensitivities $\frac{\partial|\bar{V}_i^a|}{\partial P_{13}^a}$ *with respect to active power at phase a of bus 13 as a function of the distance from the slack bus. (b) Voltage sensitivities* $\frac{\partial|\bar{V}_i^b|}{\partial P_{13}^a}$ *with respect to active power at phase a of bus 13 as a function of the distance from the slack bus*

Finally, Figures 8.8 and 8.9 depict the variation of voltage sensitivity coefficients in all the network with respect to active and reactive power absorption at phase *a* of bus 13 as a function of the distance from the slack bus.

This type of representation allows to observe the overall network behaviour against specific PQ buses absorptions/injections. In particular, we can see that larger sensitivities are observed when the distance between the considered voltage and the slack bus increases. Furthermore, a lower, but quantified dependency between coefficients related to different phases can be observed. Also, as expected, reactive power has a larger influence on voltage variations although the active power exhibits a non-negligible influence.

From the operational point of view it is worth observing that, Figures 8.8 and 8.9 provide to network operators an immediate view of the response of the electrical

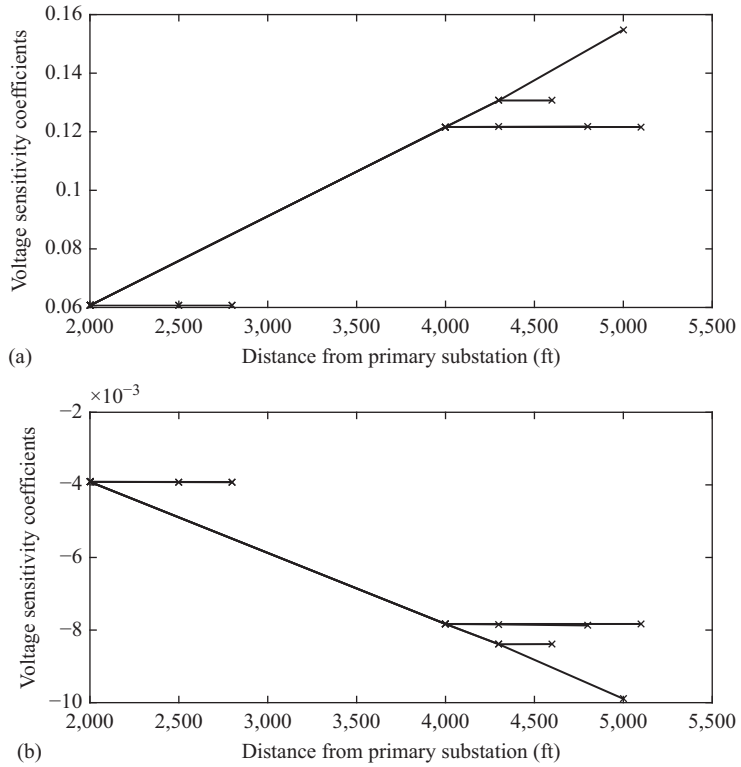

Figure 8.9 Voltage sensitivities with respect to reactive power absorption at bus 13 as a function of the distance from the slack bus. (a) Voltage sensitivities $\frac{\partial|\bar{V}_i^a|}{\partial Q_{13}^a}$ *with respect to reactive power absorption at phase a of bus 13 as a function of the distance from the slack bus. (b) Voltage sensitivities* $\frac{\partial|\bar{V}_i^b|}{\partial Q_{13}^a}$ *with respect to reactive power at phase a of bus 13 as a function of the distance from the slack bus*

network against specific loads/injections that could also be used for closed-loop control or contingency analysis.

8.4.3 Voltage control and lines congestion management examples

For the voltage control and lines congestion management application, the IEEE 34-bus test feeder is considered. Note that the regulators and shunt capacitors are excluded to make the network weaker. The network comprises a number of controllable distributed generation units. We consider three different application examples. In the first one, only voltage control is performed by coordinating the DERs' power production with the ULTC positions. In the second one, both voltage control and lines congestion management are included in the optimization problem and the control variables are

Table 8.3 Initial and maximum operational set points of the DERs and the ULTC in the IEEE 34-bus test feeder

	P_{init} (kW)	P_{max} (kW)	n_{init}	n_{min}	n_{max}
DER_{18}	210	600	0	−36	+36
DER_{23}	250	1 200			
DER_{24}	100	1 200			
DER_{33}	150	600			

solely the DERs' active and reactive power production. The third application example shows a 24 h case study of voltage control.

Example 8.1: In buses 18, 23, 24 and 33 of the IEEE 34-bus test feeder, we assume to have DERs that the DNO can control in terms of active and reactive power. Their initial operating values, as well as their rated power outputs, are shown in Table 8.3. For this case study, the loads shown in Table 8.1 are multiplied by a factor of 1.3 for phase *a*, 1.24 for phase *b* and 1.3 for phase *c*. Furthermore, the DNO has control on the transformer's ULTC positions.

In view of the above, the optimal control problem is formulated as a linearized one taking advantage of the voltage sensitivity coefficients. The controlled variables are the bus voltages and the control variables are the DER's active and reactive power injections and the ULTC positions under the control of the DNO, $\boldsymbol{\Delta x} = [\boldsymbol{\Delta P}_{DER}, \boldsymbol{\Delta Q}_{DER}, \boldsymbol{\Delta n}]$. It is important to state that, formally, this problem is a mixed integer optimization problem due to the inclusion of ULTC. However, for reasons of simplicity, in this example, the tap positions are considered pseudo-continuous variables which are rounded to the nearest integer once the optimal solution is reached. The objective of the linear optimization problem considered in this example is essentially the function in (8.1) with $\gamma = 0$ (in other words, the cost function of the optimization does not account for a deadband surrounding V_o):

$$\min_{\boldsymbol{\Delta(P,Q,n)}} \sum_i [(|\bar{V}_i| + (\boldsymbol{K}_{\boldsymbol{P,Q,n}} \boldsymbol{\Delta(P,Q,n)})_i - |V_o|)^2] \tag{8.30}$$

The imposed constraints on the operational points of the DERs and the ULTC positions are the following:

$$\begin{aligned} 0 \;&\leq\; P_{DER_i} \leq P_{DER_{i_{max}}}, \quad i = 1, \ldots, N_{DER} \\ Q_{DER_{i_{min}}} \;&\leq\; Q_{DER_i} \leq Q_{DER_{i_{max}}}, \quad i = 1, \ldots, N_{DER} \\ n_{min} \;&\leq\; n \leq n_{max} \end{aligned} \tag{8.31}$$

In order to simplify the analysis, we have assumed that the DER capability curves are rectangular ones in the PQ plane. The minimum and maximum reactive power limits are −25% and 25% of the maximum active power values, respectively.

Table 8.4 Optimal operational set points of the DERs and the tap changers in the IEEE 34-bus test feeder when the system operator has control on their three-phase output

	P_{opt_1} (kW)	Q_{opt_1} (kvar)	n_{opt_1}
DER_{18}	410.6	−150	−1
DER_{23}	1 200	−300	
DER_{24}	92.1	−300	
DER_{33}	463.2	−150	

Table 8.5 Optimal operational set points of the DERs and the tap changers in the IEEE 34-bus test feeder when the system operator has control on each of the three phases independently

	P_{opt_2} (kW)	Q_{opt_2} (kvar)	n_{opt_2}
DER_{18}^{a}	127.29	50	0
DER_{18}^{b}	50	−50	
DER_{18}^{c}	37.30	−50	
DER_{23}^{a}	50.94	100	
DER_{23}^{b}	387	−100	
DER_{23}^{c}	400	93.74	
DER_{24}^{a}	0	100	
DER_{24}^{b}	0	−100	
DER_{24}^{c}	70.71	−100	
DER_{33}^{a}	8.25	50	
DER_{33}^{b}	106.65	−50	
DER_{33}^{c}	200	−8.5	

The formulated linearized problem is solved by using the classic linear least squares method. The method used to calculate analytically the sensitivity coefficients allows us to consider two different optimization scenarios. In the first (opt_1), the operator of the system is assumed to control the set points of the DERs considering that they are injecting equal power into the three phases, whereas in the second case (opt_2), it is assumed to have a more sophisticated control on each of the phases independently except for the tap-changer positions. It is worth noting that this second option, although still far from a realistic implementation, allows us to show the capability of the proposed method to deal with the inherent unbalanced nature of distribution networks. Tables 8.4 and 8.5 show the optimal operational set points corresponding to these cases.

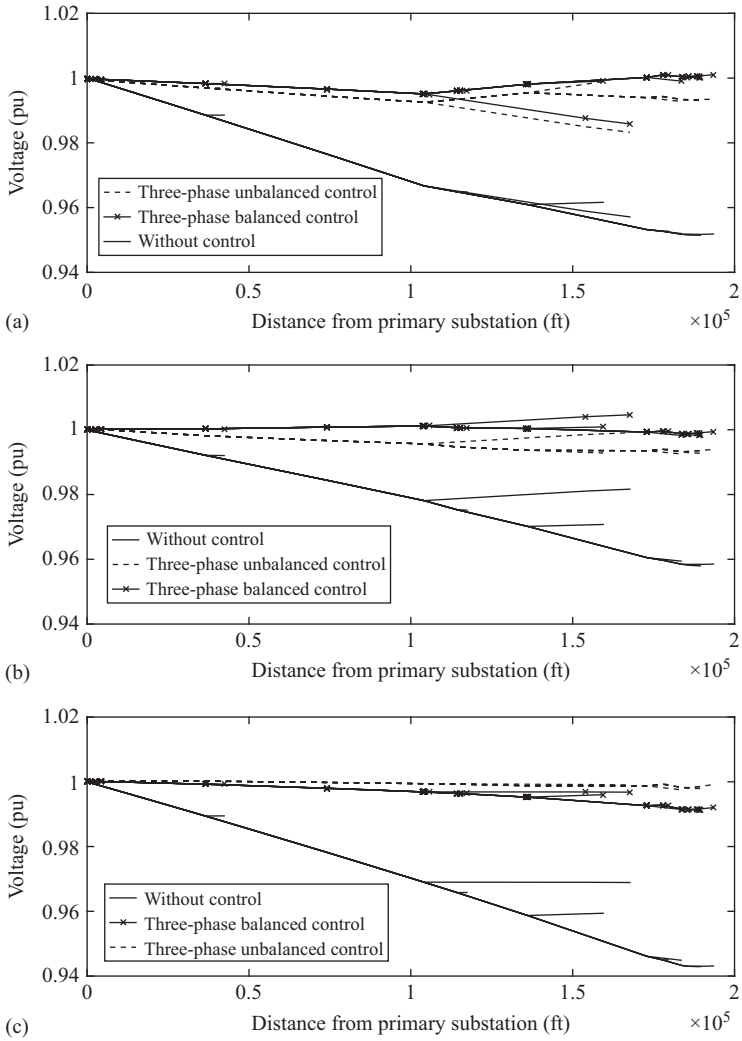

Figure 8.10 Initial and optimized voltage profile of the IEEE 34-bus test feeder. (a) Voltage profile of phase a of the buses, uncontrolled case (black solid line), balanced control (black line with markers) and three-phase unbalanced control (dashed line). (b) Voltage profile of phase b of the buses, uncontrolled case (black solid line), balanced control (black line with markers) and three-phase unbalanced control (dashed line). (c) Voltage profile of phase c of the buses, uncontrolled case (black solid line), balanced control (black line with markers) and three-phase unbalanced control (dashed line)

Table 8.6 Initial and maximum operational set points of the DERs in the IEEE 34-buss test feeder

	P_{init} (kW)	P_{max} (kW)
DER_{18}	630	1 200
DER_{23}	750	2 400
DER_{24}	300	2 400
DER_{33}	450	1 200

Additionally, in Figure 8.10, the voltage profile of the buses of the system is presented in the initial and the optimal cases. The solid line in the figures shows the initial voltage profile, the solid line with the markers shows the first case optimal scenario (opt_1) and the dashed line represents the second case where the DNO has full control in each of the phases of the DERS (opt_2). The offset in the graphs, observed in the slack bus, depicts the optimal ULTC position in each case. What can be observed is that, when there is a possibility to control each of the three phases of the DERs output, the optimal voltage profile is better than the one corresponding to control of the balanced three-phase output of the set points of the DERs.

Example 8.2: As in Example 8.1, in buses 18, 23, 24 and 33 of the IEEE 34-bus test feeder, we assume to have DERs that the DNO can control in terms of active and reactive power. Their initial operating values, as well as their rated power outputs, are shown in Table 8.6. The DERs do not inject any reactive power in the base case and their minimum and maximum reactive power limits are −25% and 25% of the maximum active power values, respectively. For this case study, the loads shown in Table 8.1 are multiplied by a factor of 1.6 for each phase *a*, *b* and *c*.

In this case, the DNO is interested to control the available distributed and centralized resources in order to improve the network voltage profile while guaranteeing that line current flows are below their ampacity limits. In this example, only three-phase balanced control of the DERs active and reactive power injections is considered and ULTC control is not taken into account. The optimal control problem is formulated as follows:

$$\min_{\boldsymbol{\Delta(P,Q)}} \sum_i [(|\bar{V}_i| + (\boldsymbol{K_{P,Q}\Delta(P,Q)})_i - |V_o|)^2 - \gamma^2]^+ \tag{8.32}$$

$$\text{subject to:} \quad |\bar{I}_{ij} + (\bar{\boldsymbol{H}}_{\boldsymbol{P,Q}}\boldsymbol{\Delta(P,Q)})_{ij}| \leq I_{max}, \quad i,j = 1,\ldots,N_l, \ i \neq j \tag{8.33}$$

$$0 \leq P_{DER_i} \leq P_{DER_{i_{max}}}, \quad i = 1,\ldots,N_{DER} \tag{8.34}$$

$$Q_{DER_{i_{min}}} \leq Q_{DER_i} \leq Q_{DER_{i_{max}}}, \quad i = 1,\ldots,N_{DER} \tag{8.35}$$

In this example, we tune the values γ and I_{max} in the optimal control problem formulation in order to evaluate the performances of the proposed method in the case of violations of the lines ampacity limits. In particular, we observe that in the base

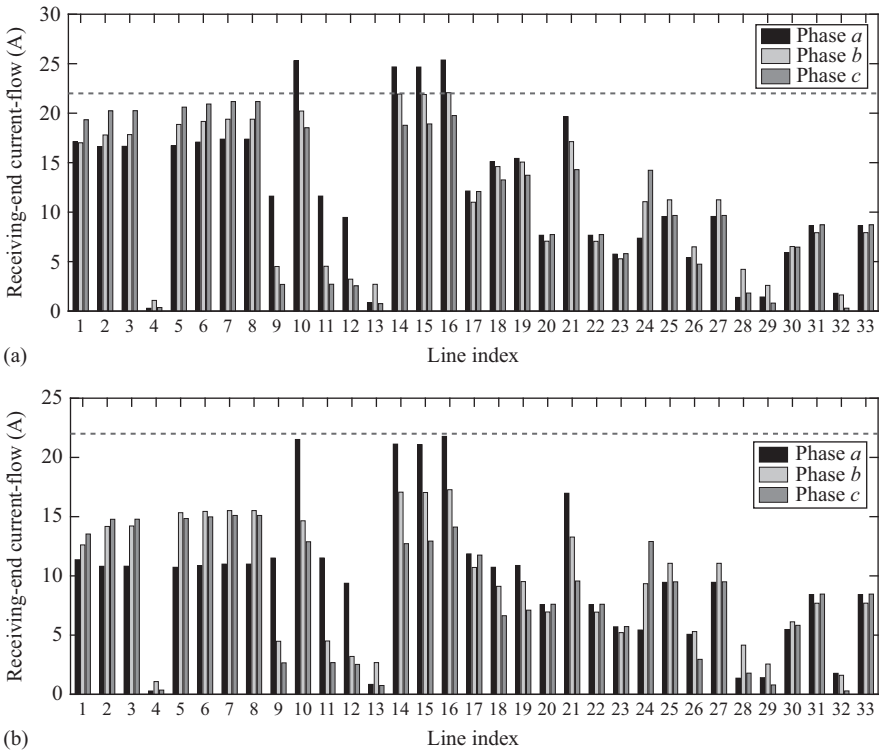

Figure 8.11 Uncontrolled and optimized lines current flows (receiving end). (a) Uncontrolled current flow at the receiving end of the network lines. (b) Optimized current flow at the receiving end of the network lines

case the maximum voltage deviation is in the order of 2% and the maximum line current flow is 25 A. Therefore, we set $\gamma = 10\%$ and $I_{max} = 20$ A to focus on the lines congestion management problem.

The results of this case study are shown in Figure 8.11 where the line current flows are shown for the receiving end of the network lines and in Figure 8.12 for the line current flows at the sending end of the lines. In both figures, on the top the uncontrolled network current profile is depicted where it can be observed that four lines violate the line ampacity limit. The same figures, on the bottom, show the results after the optimal control problem is solved. In this case, all lines satisfy, as expected, the maximum allowed current limit.

The network voltage profile for each phase is shown in Figure 8.13 before and after the control actions. In both cases, the voltage profiles are within $\pm 10\%$ of the network-rated value.

The optimal active and reactive power injections of the controllable resources for this case study are shown in Table 8.7.

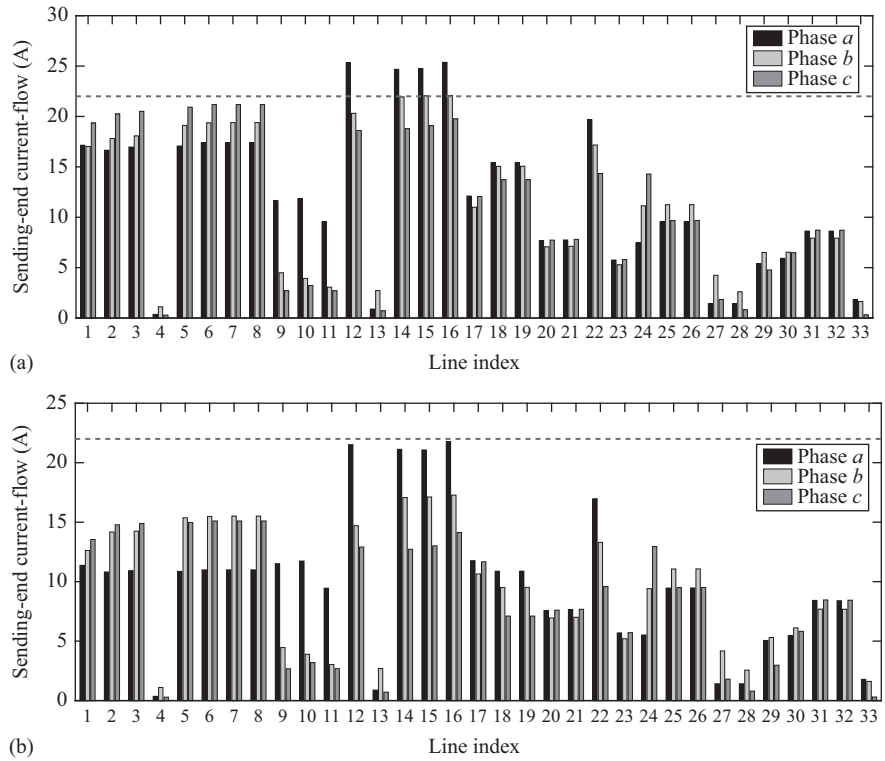

Figure 8.12 Uncontrolled and optimized lines current flows (sending end). (a) Uncontrolled current flow at the sending end of the network lines. (b) Optimized current flow at the sending end of the network lines

Example 8.3: We consider once again the IEEE 34-bus test feeder equipped with the four generators located in buses 18, 23, 24 and 33. In this example, we perform 24 h voltage control via scheduling of the active and reactive power of the DERs, as well as of the ULTCs. Only the case of balanced control is considered and lines congestion management is not taken into account.

The optimal control problem in this case is formulated as follows:

$$\min_{\boldsymbol{\Delta(P,Q,n)}} \sum_i (|\bar{V}_i| + (\boldsymbol{K_{P,Q,n}\Delta(P,Q,n)})_i - |V_o|)^2 + \psi(\boldsymbol{\Delta n})\boldsymbol{\Delta n}^2 \tag{8.36}$$

subject to:

$$0 \leq P_{DER_i} \leq P_{DER_{imax}}, \quad i = 1, \ldots, N_{DER} \tag{8.37}$$

$$Q_{DER_{imin}} \leq Q_{DER_i} \leq Q_{DER_{imax}}, \quad i = 1, \ldots, N_{DER} \tag{8.38}$$

$$n_{min} \leq n \leq n_{max} \tag{8.39}$$

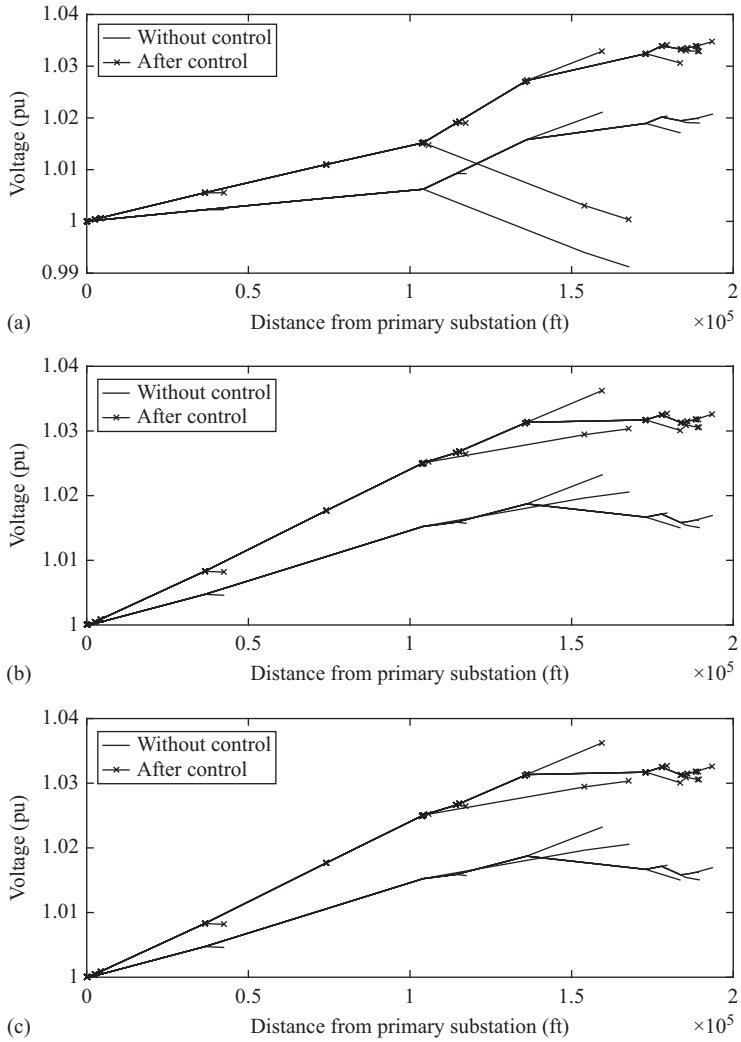

Figure 8.13 Initial and optimized voltage profile of the IEEE 34-bus test feeder. (a) Voltage profile of phase a of the buses, uncontrolled case (black solid line), balanced control (black line with markers). (b) Voltage profile of phase b of the buses, uncontrolled case (black solid line), balanced control (black line with markers). (c) Voltage profile of phase c of the buses, uncontrolled case (black solid line), balanced control (black line with markers)

Table 8.7 Optimal operational set points of the DERs

	P_{opt} (kW)	Q_{opt} (kvar)
DER_{18}	608.8	108.7
DER_{23}	729.4	109.8
DER_{24}	279.4	109.8
DER_{33}	429.4	110.0

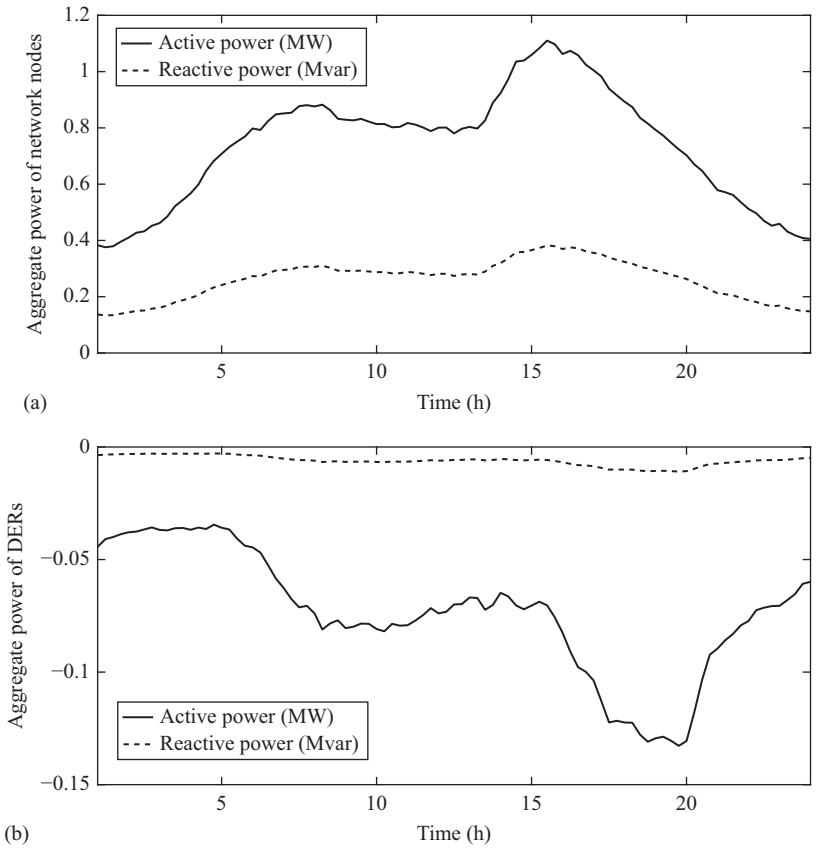

Figure 8.14 Twenty-four hour aggregate active and reactive power consumption/generation. (a) Twenty-four hour aggregate active and reactive power consumption. (b) Twenty-four hour aggregate active and reactive power generation of DERs

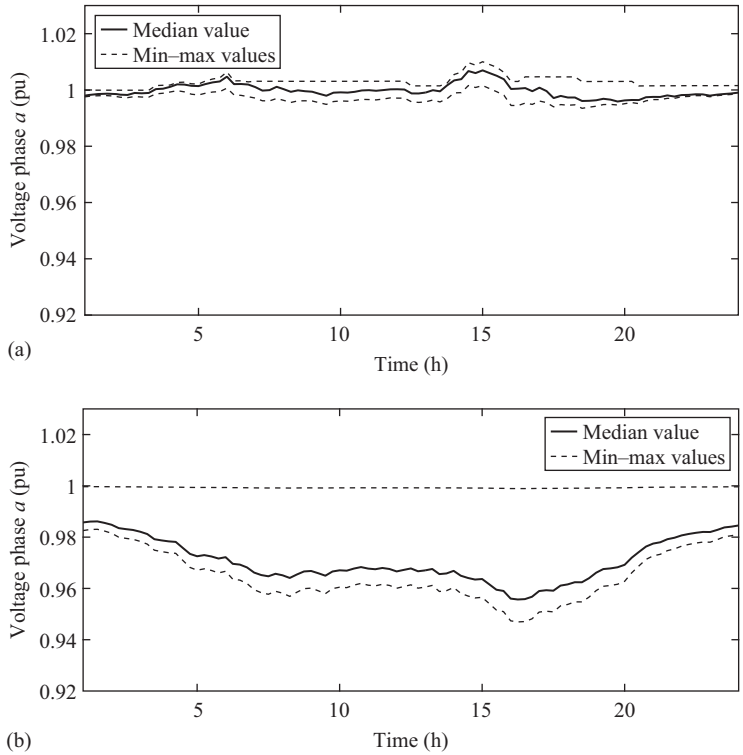

Figure 8.15 Network voltage profile of phase a before and after the control actions. (a) Uncontrolled voltage profile of phase a of the network, median value (solid line), minimum and maximum values (dashed lines). (b) Optimized voltage profile of phase a of the network, median value (solid line), minimum and maximum values (dashed lines)

where ψ is a penalty function for altering the tap-changer position.[9] The first term of (8.36) represents the voltage control cost function. The operator can perform this type of control by deploying solely the DERs or by coordinating control of the DERs and the ULTC positions. In the case where the tap changers are included, the DNO needs to account for the limited number of ULTC operations. This is represented by the term ψ of (8.36). This function multiplies the ULTC set points variation and

[9]As we deal with primary voltage control, (8.36) has to penalize the changes of ULTC as these devices are typically used by the DNO rarely.

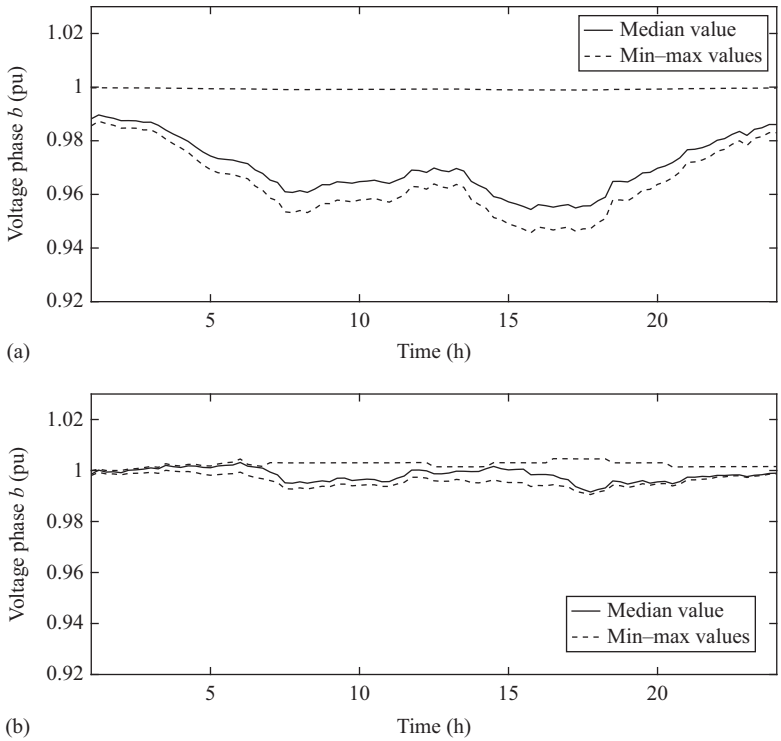

Figure 8.16 Network voltage profile of phase b before and after the control actions. (a) Uncontrolled voltage profile of phase b of the network, median value (solid line), minimum and maximum values (dashed lines). (b) Optimized voltage profile of phase b of the network, median value (solid line), minimum and maximum values (dashed lines)

increases with the number of ULTC operations in a given time window.[10] Specifically, we have chosen:

$$\psi(\boldsymbol{\Delta n}) := \lambda \left(\sum_{s=0}^{W-1} |\boldsymbol{\Delta n}(t-s)| \right) \tag{8.40}$$

where λ is a constant. Such an expression of ψ allows to weight the accumulated number of ULTC changes within a given time window W.

[10] By including this function the DNO has the option to upper-bound the total number of ULTC operations, thus respecting the nature and cost of these devices [29].

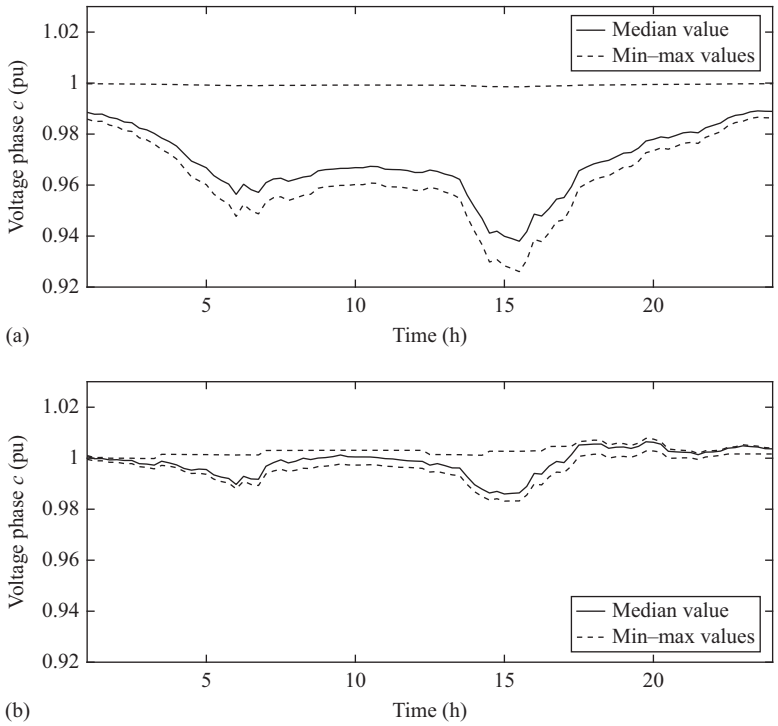

Figure 8.17 Network voltage profile of phase c before and after the control actions. (a) Uncontrolled voltage profile of phase c of the network, median value (solid line), minimum and maximum values (dashed lines). (b) Optimized voltage profile of phase c of the network, median value (solid line), minimum and maximum values (dashed lines)

For this application example, the aggregate load profile of the network is depicted in Figure 8.14 in terms of 24 h active and reactive power injections.

Figures 8.15–8.17 show, for each network phase, the 24 h voltage profile before any control action (top) and after (bottom) the scheduling of the DERs' active and reactive power and the ULTC positions. As it can be observed, the voltage profiles before the control actions are unbalanced and exhibit deviations from the network-rated value in the order of 5%–7%. After the scheduling of the controllable resources, the resulting voltage profiles for each of the three phases are flatter around 1 pu and exhibit maximum deviations from the network-rated value in the order of 1%–2%.

Figure 8.18 shows the 24 h active and reactive power output of the controllable DERs which is the result of the solution of the optimal control problem in (8.36)–(8.39), whereas Figure 8.19 shows the optimal ULTC positions along the day. It is worth noting that the obtained number of ULTC changes is compatible with a typical operation of such a device, i.e., less than 10 manoeuvres per day.

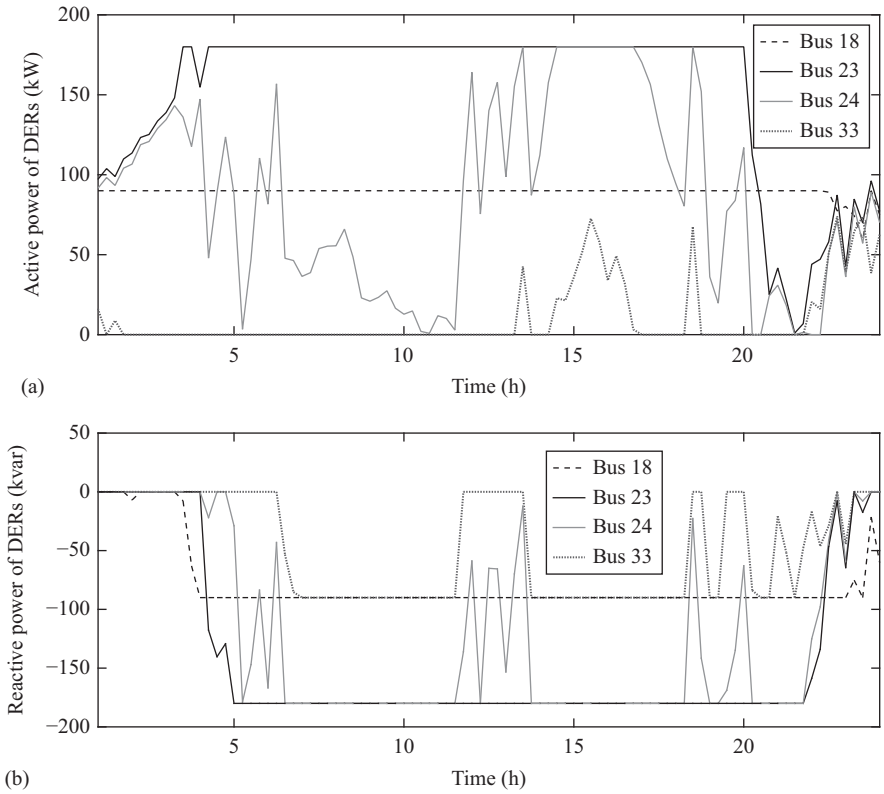

Figure 8.18 Twenty-four hour controlled active and reactive power output of the DERs. (a) Twenty-four hour three-phase active power profile of the DERs. (b) Twenty-four hour three-phase reactive power profile of the DERs

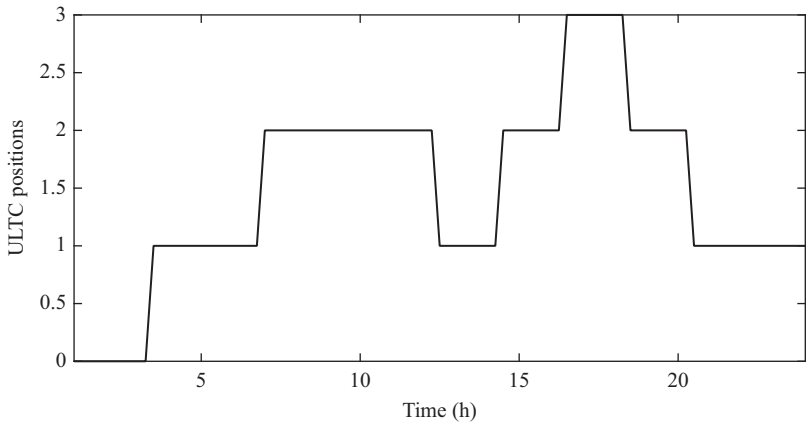

Figure 8.19 Twenty-four hour ULTC positions

8.5 Conclusions

In this chapter, we consider a centralized real-time control architecture for voltage regulation and lines congestion management in ADNs that is based on a linearized approach that links control variables (e.g., power injections and transformers tap positions) and controlled quantities (e.g., voltages and current flows) by means of sensitivity coefficients.

We validate the proposed analytic method by making reference to typical IEEE 13- and 34-bus distribution test feeders. The numerical validation of the computation of the coefficients is performed using the IEEE 13-bus test feeder and it shows that the errors between the traditional approaches, i.e., based on the inverse of the Jacobian matrix, and the analytic method are extremely low (in the order of magnitude of 10^{-6}–10^{-9}). The IEEE 34-bus test feeder is used to show application examples related to a possible integration of the proposed method for the problem of optimal voltage control and lines congestion management in unbalanced distribution systems. The simulation results show that the proposed algorithm is able to improve the voltage and current profiles in the network, and also that when each of the three phases of the DERs can be controlled independently of the others, the resulting optimal voltage and current profiles are better than the ones corresponding to the balanced control of the three-phase output of the set points of the DERs.

Bibliography

[1] Singh N, Kliokys E, Feldmann H, Kussel R, Chrustowski R, Joborowicz C. "Power system modelling and analysis in a mixed energy management and distribution management system". *IEEE Transactions on Power Systems*. 1998;13(3):1143–1149.

[2] Jenkins N, Allan R, Crossley P, Kirschen D, Strbac G. "Embedded generation". vol. 9. Johns AT, Warne DF, editors. Stevenage, UK: IET; 2000.

[3] James NG. *Control and Automation of Electrical Power Systems*. Hoboken, NJ: CRC Press; 2006.

[4] Zhou Q, Bialek J. "Generation curtailment to manage voltage constraints in distribution networks". *IET, Generation, Transmission & Distribution*. 2007;1(3):492–498.

[5] Senjyu T, Miyazato Y, Yona A, Urasaki N, Funabashi T. "Optimal distribution voltage control and coordination with distributed generation". *IEEE Transactions on Power Delivery*. 2008;23(2):1236–1242.

[6] Borghetti A, Bosetti M, Grillo S, *et al.* "Short-term scheduling and control of active distribution systems with high penetration of renewable resources". *IEEE Systems Journal*. 2010;4(3):313–322.

[7] D'adamo C, Abbey C, Baitch A, *et al.* "Development and operation of active distribution networks". *Cigré Task Force, Paris, France, Tech Brochure C*. 2011;6:1–6.

[8] Pilo F, Jupe S, Silvestro F, *et al.* "Planning and optimisation of active distribution systems: an overview of CIGRE Working Group C6. 19 activities". In: *Integration of Renewables into the Distribution Grid, CIRED 2012 Workshop*. Stevenage, UK: IET; 2012. p. 1–4.

[9] Khatod DK, Pant V, Sharma J. "A novel approach for sensitivity calculations in the radial distribution system". *IEEE Transactions on Power Delivery*. 2006;21(4):2048–2057.

[10] Conti S, Raiti S, Vagliasindi G. "Voltage sensitivity analysis in radial MV distribution networks using constant current models". In: *IEEE International Symposium on Industrial Electronics (ISIE)*. Italy: Bari, IEEE; 2010. p. 2548–2554.

[11] Czarnecki L, Staroszczyk Z. "On-line measurement of equivalent parameters for harmonic frequencies of a power distribution system and load". *IEEE Transactions on Instrumentation and Measurement*. 1996;45(2):467–472.

[12] Christakou K, LeBoudec J, Paolone M, Tomozei DC. "Efficient computation of sensitivity coefficients of node voltages and line currents in unbalanced radial electrical distribution networks". *IEEE Transactions on Smart Grid*. 2013;4(2):741–750.

[13] Bersani A, Borghetti A, Bossi C, *et al.* "Management of low voltage grids with high penetration of distributed generation: concepts, implementations and experiments". In: *Cigré 2006 Session*. EPFL-CONF-180111; 2006.

[14] Torregrossa D, Le Boudec JY, Paolone M. "Model-free computation of ultra-short-term prediction intervals of solar irradiance". *Solar Energy*. 2016;124:57–67.

[15] Sarri S, Zanni L, Popovic M, Boudec JYL, Paolone M. "Performance assessment of linear state estimators using synchrophasor measurements". *IEEE Transactions on Instrumentation and Measurement*. 2016 Mar;65(3):535–548.

[16] Camacho EF, Alba CB. *Model Predictive Control*. Berlin: Springer Science & Business Media; 2013.

[17] Ben-Tal A, El Ghaoui L, Nemirovski A. *Robust Optimization*. Princeton, NJ: Princeton University Press; 2009.

[18] Sarri S, Paolone M, Cherkaoui R, Borghetti A, Napolitano F, Nucci CA. "State estimation of active distribution networks: comparison between WLS and iterated Kalman-filter algorithm integrating PMUs". In: *Third IEEE PES Innovative Smart Grid Technologies (ISGT) Europe Conference*. Germany: Berlin, 2012.

[19] Pegoraro PA, Tang J, Liu J, Ponci F, Monti A, Muscas C. "PMU and smart metering deployment for state estimation in active distribution grids". In: *Energy Conference and Exhibition (ENERGYCON), 2012 IEEE International*. Italy: Florence, 2012. p. 873–878.

[20] De Carne G, Liserre M, Christakou K, Paolone M. "Integrated voltage control and line congestion management in active distribution networks by means of smart transformers". In: *Industrial Electronics (ISIE), 2014 IEEE 23rd International Symposium on Industrial Electronics (ISIE)*. Turkey: Istanbul, 2014. p. 2613–2619.

[21] Peschon J, Piercy DS, Tinney WF, Tveit OJ. "Sensitivity in power systems". *IEEE Transactions on Power Apparatus and Systems*. 1968;(8):1687–1696.
[22] Shirmohammadi D, Hong H, Semlyen A, Luo G. "A compensation-based power flow method for weakly meshed distribution and transmission networks". *IEEE Transactions on Power Systems*. 1988;3(2):753–762.
[23] Wood AJ, Wollenberg BF. *Power Generation, Operation, and Control*, vol. 2. New York, NY: Wiley; 1996.
[24] Marconato R. *Electric Power Systems*, vol. 2. Milano, Italy: CEI, Italian Electrotechnical Committee; 2002.
[25] Begovic MM, Phadke AG. "Control of voltage stability using sensitivity analysis". *IEEE Transactions on Power Systems*. 1992;7(1):114–123.
[26] Christakou K, Tomozei DC, Bahramipanah M, Le Boudec JY, Paolone M. "Primary voltage control in active distribution networks via broadcast signals: the case of distributed storage". *IEEE Transactions on Smart Grid*. 2014 Sep;5(5):2314–2325.
[27] Arrillaga J, Bradley D, Bodger P. *Power System Harmonics*. New York, NY: John Wiley; 1985.
[28] Kersting WH. "Radial distribution test feeders". *IEEE Transactions on Power Systems*. 1991 Aug;6(3):975–985.
[29] Virayavanich CHKWS, Seiler A. "Reliability of on-load tap changers with special consideration of experience with delta connected transformer windings and tropical environmental conditions". In: *Cigré, Paper*; 1996. p. 12–103.